



Experimental and DFT Computational Insights on the Adsorption of Selected Pharmaceuticals of Emerging Concern from Water Systems onto Magnetically Modified Biochar

Umar Yunusa^{1*}  , Umaru Umar¹ , Sulaiman Adamu Idris² , Abdulrahman Ibrahim Kubo³ 
and Tahir Abdullahi⁴ 

¹ Department of Pure and Industrial Chemistry, Bayero University, Kano-Nigeria

² Department of Science Laboratory Technology, Federal Polytechnic Offa, Kwara-Nigeria

³ Department of Pure and Applied Chemistry, Adamawa State University, Mubi-Nigeria

⁴ Department of Physics, Yobe State University, Damaturu-Nigeria

Abstract: This work aimed to fabricate a magnetically modified biochar (MBC) through a one-step pyrolysis of *Vitex doniana* nut at 500 °C and investigate its feasibility for the removal of two pharmaceuticals, namely, amoxicillin (AMX) and trimethoprim (TMT) from aqueous environment. The textural characteristics, chemical composition and magnetic properties of the MBC were analyzed using Brunauer-Emmett-Teller (BET) analysis, scanning electron microscopy (SEM), Fourier Transform Infrared (FTIR) spectroscopy, X-ray diffraction (XRD) and vibrating sample magnetometer (VSM). The results demonstrated the successful incorporation of the magnetic particles in the biochar matrix. The specific surface area and average pore volume of the MBC were obtained as 108.90 m²/g and 2.98 cm³/g, respectively. The adsorption process was observed to be strongly pH-dependent, and equilibrium was attained within 1 h. The kinetic data favors pseudo-second-order model ($R^2 > 0.999$), implying that the most plausible mechanism for the adsorption was chemisorption. The isothermal data was best fitted by the Langmuir model ($R^2 > 0.985$), signifying that the process was mainly monolayer adsorption on homogeneous surface. The maximum adsorption capacity achieved for AMX and TMT was 41.87 and 55.83 mg/g at 303 K, respectively. The thermodynamic examination highlighted that the adsorption was feasible and accompanied with absorption of heat and increase of entropy for both the adsorbates. Furthermore, the MBC exhibited a good recycling capability such that the adsorption capacity decreases by ~ 25% after reuse for six cycles. Besides, the theoretical results based on density functional theory (DFT) calculations demonstrated that the TMT molecules ($\Delta E = 3.762$ eV) are more reactive compared to the AMX molecules ($\Delta E = 3.855$ eV) which correlates with the experimental observations.

Keywords: Adsorption, pharmaceuticals, *Vitex doniana*, magnetic biochar, DFT calculations.

Submitted: March 20, 2021. **Accepted:** October 25, 2021.

Cite this: Yunusa U, Umar U, Idris S, Kubo A, Abdullahi T. Experimental and DFT Computational Insights on the Adsorption of Selected Pharmaceuticals of Emerging Concern from Water Systems onto Magnetically Modified Biochar. JOTCSA. 2021;8(4):1179–96.

DOI: <https://doi.org/10.18596/jotcsa.900197>.

***Corresponding author. E-mail:** umaryunusa93@gmail.com.

INTRODUCTION

Over the last few decades, many classes of micro-pollutants including pharmaceuticals, steroid hormones, pesticides, endocrine disrupting compounds, and personal care products have been detected in various freshwater resources worldwide. Among them, pharmaceuticals have emerged as one of the major concerns of public health authorities (1,2). The drug industries, hospitals, and households are the main sources of pharmaceutical contaminants in water systems (3). Most compounds of pharmaceutical origins are persistent, non-biodegradable and often not appreciably eliminated due to their ability to pass through the treatment processes largely undisturbed (4). Therefore, their residues are rampant in surface water, partially treated water and groundwater, typically at trace quantities from ng/L to µg/L. Long-term exposure to pharmaceuticals may pose a deleterious risk to humans and has been established to have significant disruptive impacts in aquatic ecosystems (5). To date, the treatment of pharmaceuticals has been a daunting task due to their complex physicochemical properties.

Numerous decontamination technologies have been employed to eliminate pharmaceutically active compounds from aqueous medium including coagulation, biological treatment, adsorption, filtration, and advanced oxidation processes. However, the efficiencies of these traditional processes such as filtration, coagulation and biodegradation were insufficient. In contrast, advanced oxidation processes are also not easily applicable in industrial scale owing to expensiveness of energy and the generation of undesired byproducts. In this regard, adsorption appears to be favorite alternative due to its effectiveness, low-cost of operation and complete elimination of the pharmaceutical without causing any secondary pollution (6).

The use of carbon-based materials is the most prominent method for removal of organic contaminants from water streams. Biochar is a carbon-rich material produced mainly from the carbonization of biomass feedstock in an oxygen-depleted medium. The preparation of biochar does not require the activation process and uses less energy (7). Although biochar in their ordinary forms have been employed as solid adsorbents, they suffer from limitations such as small particle size, poor adsorption performance, and ability of separation from bulk solution (8). Therefore, it is imperative to modify biochars in order to enhance their adsorption efficiency towards pollutants. Recently, magnetic modification has seen tremendous interest as a remedy to overcome these shortcomings. Magnetic

response is attained through functionalization of biochar surface with magnetic particles such as magnetite and maghemite (9). High adsorption performance, easy to separate from water, reuse potential, and natural abundance of precursors are the main attributes which promote magnetic biochar as a promising adsorbent for the removal of various pollutants.

Vitex doniana (VD), also known as black plum, is one of the most abundant trees present in tropical Africa. The plant has emerged as a priority species because of the multiplicity of its uses. For instance, the plant is extensively used for food, source of timber and for medical purposes (10). The *Vitex doniana* nut is the major waste generated from processing of this plant and most are discarded on the fields. Few studies have reported the use of this plant's leaves and nut as adsorbents for the elimination of toxic metals (11,12). Nevertheless, to the best of our knowledge, no work has been reported so far on the preparation of biochar from *Vitex doniana* nut and its application for the removal of medicinal drugs from water.

In this regard, two pharmaceuticals, amoxicillin (AMX) and trimethoprim (TMT) were chosen as the model pollutants for this study. The selection of these two antibiotics was based on the frequency of occurrence in freshwater resources. Moreover, information on their removal from aquatic environment is relatively scarce. TMT is among the most prominent antibiotics employed in veterinary and human medicine worldwide acting as an inhibitor in the chemotherapy treatment (13). AMX belongs to a class of drugs that are majorly excreted in a non-metabolized form, and some reports have highlighted that AMX might pose an acute risk to the aquatic ecosystem (14,15).

With this background, the overall objective of this research is to investigate the adsorption of amoxicillin and trimethoprim molecules on the surface of magnetically modified biochar derived from *Vitex doniana* nut wastes. To achieve this objective, the influence of experimental factors such as pH, ionic strength, temperature, initial concentration, and contact time on the adsorption capacity of the adsorbent was studied. Additionally, the removal process was assessed isothermally, thermodynamically, and kinetically in order to gain insight about the mechanism and spontaneity of adsorption. Finally, density functional theory (DFT) computations were performed to obtain qualitative insights on the chemical reactivity of amoxicillin and trimethoprim molecules.

EXPERIMENT AND COMPUTATION

Chemicals and Materials

Amoxicillin and Trimethoprim were obtained from Sigma-Aldrich (USA). Their physicochemical properties are depicted in Table 1. Ferric chloride ($\text{FeCl}_3 \cdot 6\text{H}_2\text{O}$), sodium nitrate (NaNO_3) and other chemicals used were AnalaR grade sourced from Fisher Chemicals (USA). *Vitex doniana* nut was acquired from Kano State, Nigeria. Demineralized water was employed during the entire adsorption tests.

Preparation of Magnetically Modified Biochar

Vitex doniana nuts were cut into small pieces, washed, and then subsequently dried at 110 °C for 48 h. The dried nut was pulverized and sieved into desirable particle sizes (≤ 1 mm) and subsequently heated in a muffle furnace from room temperature to 500 °C for 3 h. The process of pyrolysis was performed at a heating rate of 10 °C/min and under an oxygen-depleted condition. After pyrolysis, the resulting biochar was collected from the furnace after being cooled to room temperature. Then 10 g of the obtained biochar was immersed into a mixed solution containing 4 g of $\text{FeCl}_2 \cdot 2\text{H}_2\text{O}$ and 8 g $\text{FeCl}_3 \cdot 6\text{H}_2\text{O}$ in 50 mL of demineralized water. The obtained mixture was homogenized by vigorous stirring for 10 h at 90 °C. The precipitation of iron oxide particles on the biochar was achieved by the addition of drops of 10 mL NH_4OH solution into the mixture with the aid of rapid stirring for 30 min at 90 °C. After that, the stable suspension was cooled to room temperature. Finally, the produced magnetically modified biochar (MBC) was retrieved from the mixture using external magnet. The MBC was washed repeatedly with demineralized water to attain pH 7.0, and then dried in oven at 50 °C for 24 h.

Determination of Characteristics of the Magnetic Biochar

Surface functional group characteristics of the MBC was elucidated using FTIR spectrometer (Cary 630; Agilent Technologies) in the 4000-650 cm^{-1} wave number range under a resolution of 8 cm^{-1} , while the crystallographic structure was analyzed using XRD (Rigaku Ultima IV) with a Cu K α radiation in the 2θ range of 5-85°. The surface texture of the MBC was examined by means of electron microscopy utilizing a scanning electron microscope (JEOL-JSM6480). The BET surface area was measured using a specific surface area and pore size analyzer (BET, Builder, SSA-4300). Magnetic properties of MBC was assessed at 298 K using a vibrating sample magnetometer (VSM, EV9) with a maximum applied magnetic field of 15 kOe. The influence of varying pHs over the surface charge was probed via determination of the point of zero charge, pH_{pzc} . The pH_{pzc} is the pH value in which

MBC surface presents a net electrical neutrality. A pH_{pzc} of 6.9 was obtained following a salt addition method described in the literature (16). More precisely, 0.2 g of MBC sample was added to 40 mL of 0.1 M NaNO_3 solution in a centrifuge tube. The medium pH was adjusted to a value between 2 and 11 by addition of dilute HCl or NaOH solutions. All solutions were stirred continuously for 24 h and the final pH was recorded. A graph between the changes in pH (ΔpH) was plotted against the initial pH and the intersection point was taken as pH_{pzc} .

Experimental Protocol of Pharmaceuticals' Adsorption

A known mass of MBC (0.1 g) was mixed with 100 mL of aqueous pharmaceutical solution of known concentrations in series of 250 mL Erlenmeyer flasks placed on thermostatically controlled incubator shaker. The mixture was agitated at 150 rpm for pre-decided residence times. 0.1 M NaOH or 0.1 M HCl solutions were used as pH adjusters to desired value. After the adsorption process, the spent adsorbent was retrieved by an external magnet, and about 3 mL of the solution was transferred to the cuvette and analyzed by the procedure highlighted in subsequent section. Each experiment was run at least in triplicate and the mean values were adopted in the report. Relative standard deviation is not reported as it is negligible (<2%).

The effect of pH on the AMX and TMT uptake was evaluated with initial solution pH varying from 2 to 10. The tests for effect of ionic strength were implemented at varying NaCl concentrations (0.05 to 0.15 mol/L). The influence of contact time (kinetic study) was assessed from 5 min up to 120 min. Equilibrium experiments (isotherm study) were carried out at initial concentrations ranging from 20 to 100 mg/L. The impact of temperature (thermodynamic study) on the adsorption process was evaluated from 303 to 333 K.

Regeneration and Reuse

The MBC was cleaned after adsorption of AMX and TMT using demineralized water and acetone. Briefly, 0.1 g of MBC was placed into 50 mL of acetone. The mixture was agitated in an incubator shaker maintained at 150 rpm under room temperature (30 ± 1 °C) for 12 h. Afterward, the regenerated adsorbent was washed with demineralized water and dried at 90 °C. The adsorbent was used to assess the adsorption capacities up to six cycles.

Quantification of Amoxicillin and Trimethoprim in Aqueous Solution

The quantitative determination of AMX and TMT was accomplished by UV-visible spectrophotometry. The absorbance of the pharmaceutical solutions was

recorded by UV-visible spectrophotometer (Lambda 35; Perkin Elmer) at a characteristic wavelength of 228 nm for AMX and 275 nm for TMT. Calibration curves were established using solutions of each pharmaceutical in demineralized water in a range of 1-10 mg/L. The calibration curves for both the adsorbates exhibited an excellent linearity ($R^2 > 0.99$).

The adsorption performance of the MBC was assessed through the parameter q , (mg of pharmaceuticals adsorbed per gram of MBC), as expressed in Equation 1:

$$q = \frac{C_0 - C_f}{m} \times V \quad (1)$$

where C_0 stands for initial pharmaceutical concentration (mg/L), C_f represent the pharmaceutical concentration at any time given (mg/L), V reflects the volume of the experimental solution in liters, and m denotes the weight of the MBC used in grams.

Adsorption Modelling

The kinetics of the adsorption of the pharmaceuticals onto the MBC was assessed by conducting the time-dependent studies. Many kinetics models, viz., pseudo-first-order (PFO), pseudo-second-order (PSO) and intraparticle diffusion (IPD) models were employed to interpret the experimental data. The PFO, PSO and IPD models in their linear form are represented by Eqs. 2, 3, and 4, respectively:

$$\log(q_e - q_t) = \log q_e - k_1 t \quad (2)$$

$$t/q_t = 1/(k_2 q_e^2) + t/q_e \quad (3)$$

$$q_t = k_{id} t^{(1/2)} + C \quad (4)$$

where q_e and q_t represent the adsorption capacity of the MBC at the equilibrium state and at time of t , respectively; k_1 (min^{-1}), k_2 (g/mg min) and k_{id} denote the moduli of PFO, PSO and IPD adsorption, respectively.

The equilibrium data were adjusted to the Langmuir and Freundlich models. The linear expressions of these models are illustrated by Equations 5 and 6, respectively:

$$C_e/q_e = 1/(K_L q_{max}) + C_e/q_{max} \quad (5)$$

$$\ln q_e = \ln [K_F] + \ln(1)/n \ln C_e \quad (6)$$

where C_e (mg/L) is the equilibrium concentration of pharmaceuticals, q_e (mg/g) is the amount of

pharmaceuticals adsorbed per gram of MBC under equilibrium, q_{max} (mg/g) is the theoretical monolayer adsorption capacity of MBC for pharmaceuticals, and K_L (L/mg) is a constant pointing the affinity in the Langmuir adsorption process; K_F is the Freundlich empirical constant representing the relative adsorption capacity of the MBC, and n (dimensionless) is a constant illustrative of the intensity of the Freundlich adsorption.

Validity of Models

The capability of the studied kinetic models in fitting the experimental data and the suitability of the investigated isotherms in describing the behavior of the adsorptive system was validated through coefficient of determination (R^2), chi square (χ^2) and sum squares of errors (SSE, %). These error functions can be represented by Eqs. 7-9, respectively (17):

$$R^2 = 1 - \frac{(\sum (q_{(e,exp)} - q_{(e,model)})^2)}{(\sum (q_{(e,exp)} - q_{(e,mean)})^2)} \quad (7)$$

$$\chi^2 = \sum \frac{(q_{(e,exp)} - q_{(e,model)})^2}{q_{(e,model)}} \quad (8)$$

$$SSE (\%) = \frac{\sqrt{(\sum (q_{(e,exp)} - q_{(e,model)})^2)}}{N} \quad (9)$$

where $q_{e,model}$ and $q_{e,exp}$ (mg/g) represent the model predicted and experimental uptake capacity, respectively; $q_{e,mean}$ denotes the mean of the $q_{e,exp}$ values; and N is the number of data points. The best fitting model exhibits the highest value of R^2 , but the lowest value of SSE and χ^2 .

Computational Methods

The molecular structures of the pharmaceuticals were designed using ChemDraw Ultra 7.0 software. Then the structures were imported for DFT calculations using the Materials Studio 8.0 software package (BIOVIA, Accelrys). The optimization of the full molecular geometry of AMX and TMT was implemented using DMol³ module at the level B3LYP/DND. No symmetry constraints were imposed during the geometrical optimization of the tested molecules. The quantum chemical parameters were estimated from energies associated with frontier molecular orbitals [the highest occupied molecular orbital (HOMO; E_H), lowest unoccupied molecular orbital (LUMO; E_L), and an energy gap ($\Delta E = E_H - E_L$), electron affinity ($A = -E_L$), and ionization potential ($I = -E_H$). The global reactivity indexes namely, chemical potential (μ), chemical hardness (η), chemical softness (σ) electronegativity (χ) and global electrophilicity power (ω), were approximated

in terms of Frontier orbital energies as expressed by Equations 10-14, respectively (18):

$$\mu = \frac{(E_H + E_L)}{2} \quad (10)$$

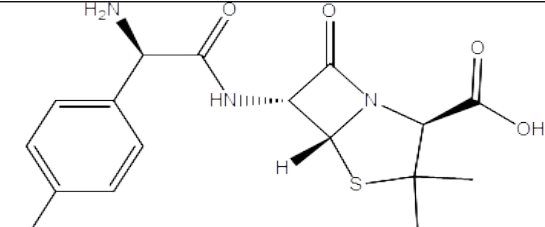
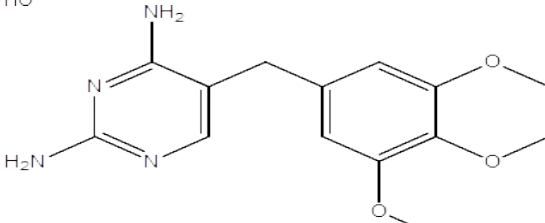
$$\eta = \frac{(E_L - E_H)}{2} \quad (11)$$

$$\sigma = \frac{1}{\dot{\eta}} \quad (12)$$

$$\chi = \frac{(I + A)}{2} \quad (13)$$

$$\omega = \frac{\mu^2}{2\dot{\eta}} \quad (14)$$

Table 1: Target pharmaceuticals and their characteristics.

Pharmaceutical	Molecular Structure	MW (g/mol)	pKa
Amoxicillin		365.4	3.2 (carboxyl) 11.7 (amine)
Trimethoprim		290.3	7.1

RESULTS AND DISCUSSION

Characterizations

SEM micrographs clearly depicting the morphological characteristics of the native and modified biochar are presented in Figure 1. As can be seen in Figure 1a, the micrograph revealed the rough and heterogeneous nature of the biochar surface. After magnetic modification, the SEM micrograph depicts a relatively porous flower-like structure on the surface, demonstrating that the surface structure of MBC is different from those of native biochar, presumably due to the presence of Fe particles (Figure 1b). This indicates that the modification of the biochar enhances the porosity of the material, and thus can facilitate the penetration and binding of the pharmaceuticals.

The Brunauer–Emmett–Teller (BET) analysis was performed to determine the specific surface area and pore size of the adsorbent. The results showed that the magnetic modification of the biochar led to an increase in specific surface area from 96.31 m²/g for the native biochar to 108.90 m²/g for the MBC. This signifies that the MBC has a remarkable potential to adsorb the target adsorbates. Meanwhile, the average

pore volume (VP), and pore diameter were found to be 0.55 cm³/g and 1.17 nm, respectively, for biochar and 2.98 cm³/g and 0.76 nm, respectively, for MBC. The change in the textural properties may be ascribed to the decoration of biochar with magnetic particles.

The XRD profile of MBC (Figure 2) revealed the diffraction peaks at 2θ = 30.7° (220), 35.6° (311), 43.5° (400), 57.3° (511) and 62.9° (440), which was associated with the standard XRD data of γ-Fe₂O₃ and Fe₃O₄ spinel structure (19,20). The sharp diffraction peaks suggest that the as-synthesized iron oxides were incorporated into the biochar matrix (21). The difference between the two magnetic iron oxides is not feasible by XRD since their diffraction peaks are very similar. But, it is safe to state that γ-Fe₂O₃ and Fe₃O₄ are the major crystalline components present in MBC.

The surface functional groups of MBC that might participate in pharmaceuticals adsorption are elucidated by FTIR analysis (Figure 3). An obvious band centered at around 3409 cm⁻¹ was ascribed to the O–H and –NH₂ stretching vibration (22). The peak at around 1628 cm⁻¹ was attributed to C=C stretching vibrations of aromatic ring. The bands observed in the

range of $1000\text{-}1200\text{ cm}^{-1}$ may be assigned to stretching vibration of C-O- (ether or alcohol) and -N-H, signifying the presence of diverse functional groups (23). Lastly, a weak peak at 579 cm^{-1} can be assigned to Fe-O bonds vibrations compatible with the presence of $\gamma\text{-Fe}_2\text{O}_3$ and Fe_3O_4 (20). The aforementioned result further affirmed that iron oxide was successfully incorporated into the biochar matrix. Characteristics of infrared spectra of blank MBC and adsorbate-loaded MBC are also contrasted in Figure 3. Some slight changes in peak positions were observed after adsorption which signify the interactions between the pharmaceuticals and MBC's surface functional groups.

The magnetic properties of the adsorbent was recorded at the magnetic fields of $-15000\leq H\leq 15000$ Oe at 298K. As presented in Figure 4, the MBC displayed appreciable saturation magnetization (M_s) value of 7.70 emu/g . This was attributed to the presence of iron oxides particles on the biochar surface. The $\text{Fe}_3\text{O}_4/\gamma\text{-Fe}_2\text{O}_3$ particles loaded on the adsorbent surface exhibit magnetic properties, which in turn render the biochar magnetically active (24). Moreover, the magnetization curve suggested that the adsorbent was ferromagnetic, attesting the potential for easy retrievability and reusability through magnetic recovery.

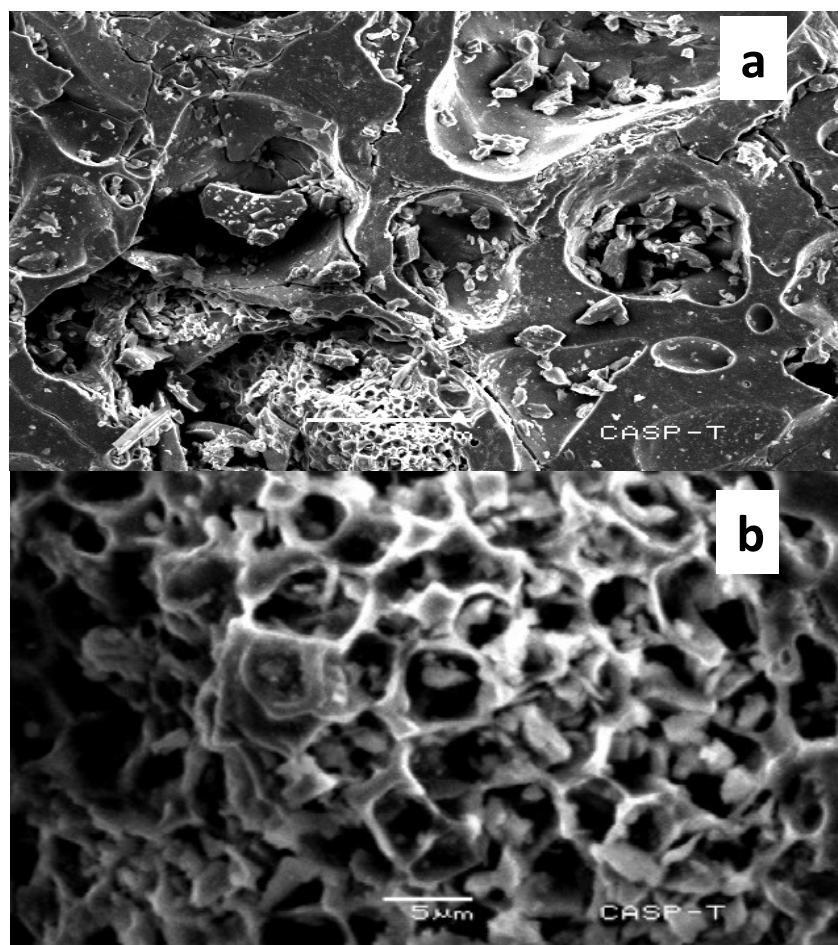


Figure 1: SEM images of (a) biochar (b) MBC.

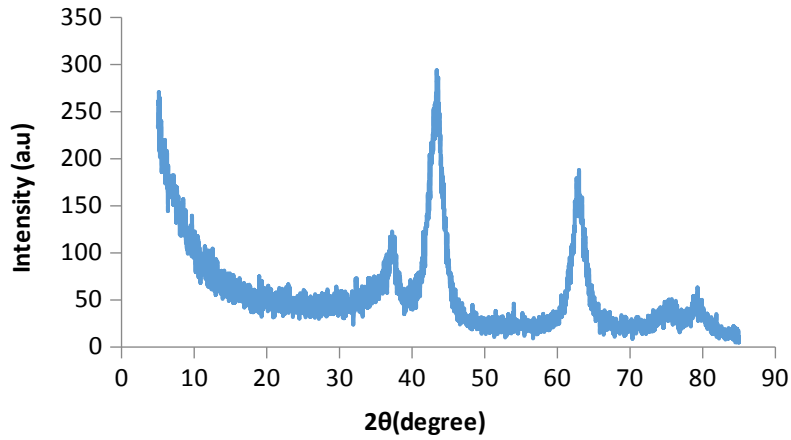


Figure 2: XRD pattern of MBC.

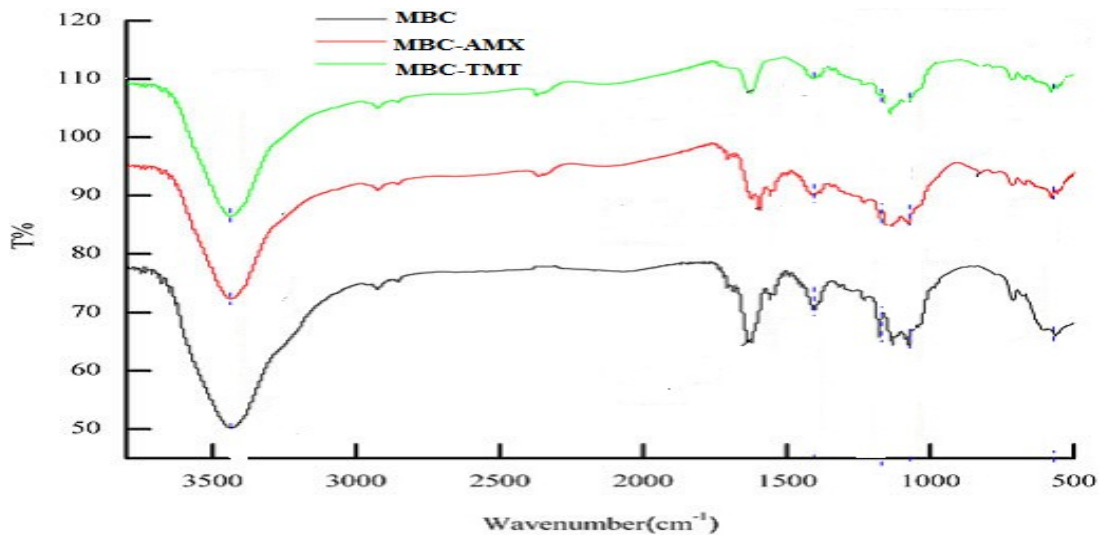


Figure 3: FTIR spectra of the MBC before and after adsorption of AMX and TMT.

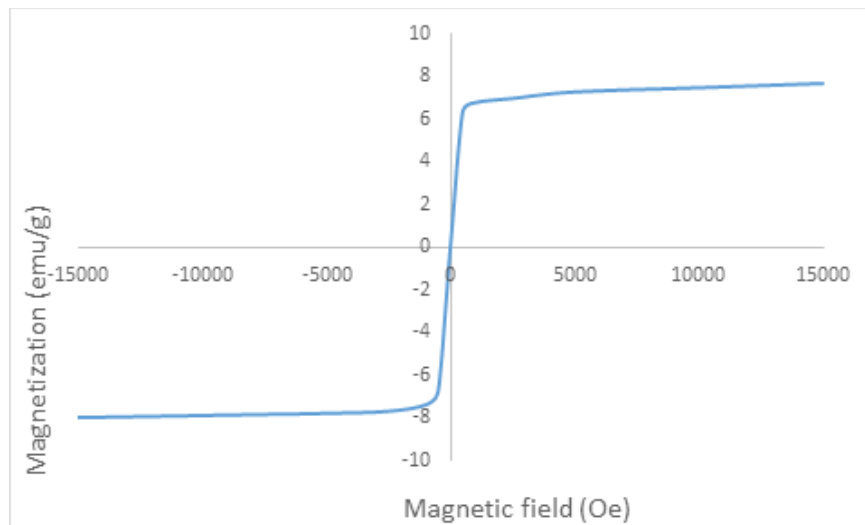


Figure 4: Magnetic hysteresis curve of MBC.

Study of the Effects of pH and Ionic Strength

Due to discrepancy in the values of acid dissociation constants (pK_a) of the examined pharmaceuticals, it is anticipated that both AMX and TMT could yield different charges under varying experimental conditions. As can be observed in Figure 5, the adsorption potential of AMX appreciably increases with a decrease in the pH, and maximum uptake was observed at $pH = 3$. However, TMT exhibited a different behavior from the AMX as the decrease in pH resulted in a lower adsorption yield and the optimum condition was presented at $pH = 8$. The distinct behavior of the adsorption of the pharmaceuticals can be explained by considering the electrostatic interactions between the examined adsorbates and target adsorbent. For $pH < p_{H_{pzc}}$, the surface of the MBC is positively charged, while for $pH > p_{H_{pzc}}$, the adsorbent bears a negative charge at its surface. The solution pH also determines the appearances of charges in the examined pharmaceuticals, therefore, both attractive and repulsive interactions could be induced. The high adsorption of AMX in acidic

environment may be explained by considering the ionization of the carboxyl group ($pK_a = 3.2$). It is obvious that the pK_a value of the aliphatic carboxylic acid functionality of AMX is close to pH 3. Therefore, this group is not completely protonated carrying partial negative charges that could enhance electrostatic attraction between the AMX and MBC (25). By contrast, TMT performs better in basic medium, having a similar pK_a (7.1) to the pH_{pzc} (6.9) which induces greater repulsion in low pHs (26).

Since there are many types of ions in different wastewaters, it seems imperative to investigate ionic strength's influence on the adsorption process. To achieve this, sodium chloride (NaCl) salt was used for adjusting the ionic strength of the adsorbates' solution. As shown in Figures 6 and 7, the adsorption capacity of MBC for both AMX and TMT decreases slightly with increasing ionic strength of the solution. This indicates that the salt concentration has an insignificant influence on the adsorption of AMX and TMT onto the MBC.

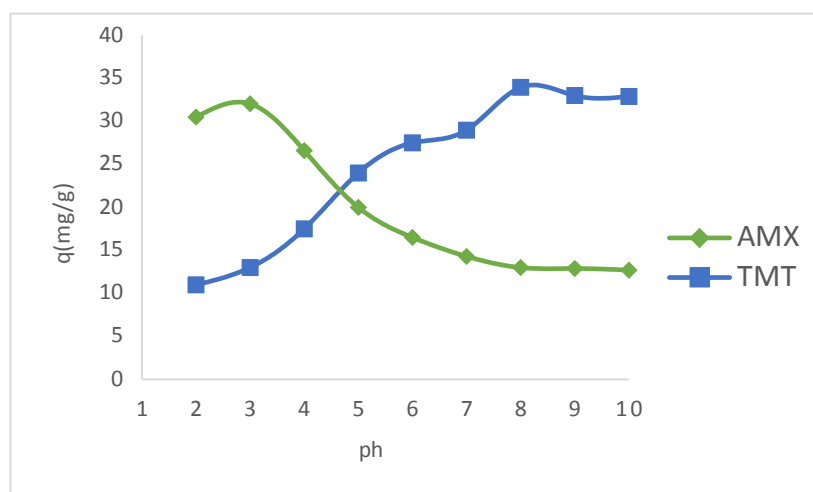


Figure 5: Effect of pH on the adsorption of AMX and TMT onto MBC (Conditions: $pH = 2-10$; contact time = 60 min; adsorbent weight = 0.1 g; $C_0 = 60$ mg/L, solution volume = 100 mL and temperature = 303 K).

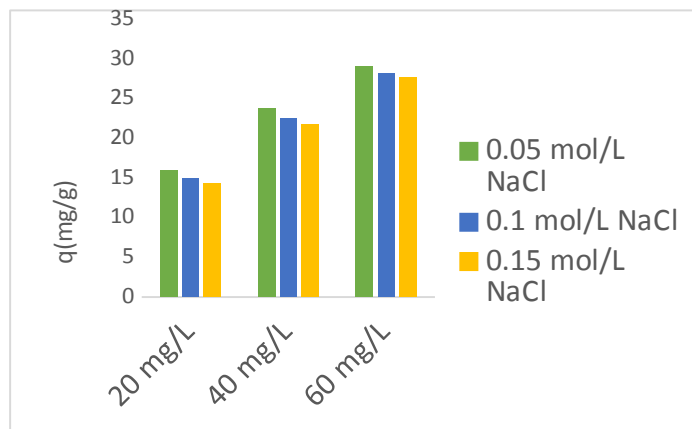


Figure 6: Effect of ionic strength on AMX adsorption by MBC at different initial concentration (Conditions: salt concentration = 0.05-0.15 mol/L; pH = 3; contact time = 60 min; adsorbent weight = 0.1 g; C_o = 20-60 mg/L, solution volume = 100 mL and temperature = 303 K).

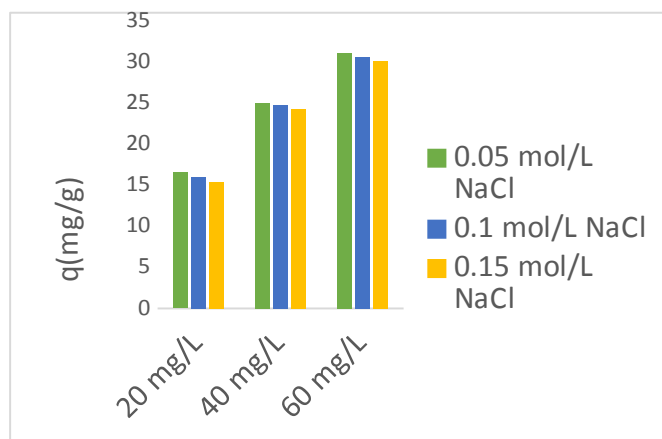


Figure 7: Effect of ionic strength on TMT adsorption by MBC at different initial concentration (Conditions: salt concentration = 0.05-0.15 mol/L; pH = 8; contact time = 60 min; adsorbent weight = 0.1 g; C_o = 20-60 mg/L, solution volume = 100 mL and temperature = 303 K).

Adsorption Kinetics

The impact of contact time on the adsorption process of AMX and TMT onto MBC was presented in Figure 8. It can be seen that the adsorption process attained a relatively fast equilibrium at around 60 min of residence time, suggesting that the MBC surface had a high affinity towards the pharmaceutical molecules in solution.

The values of kinetic parameters for the adsorption of pharmaceuticals onto the MBC as evaluated from the curve-fitting graphs (Figures 9 and 10) are presented in Table 2. An excellent agreement between the theoretical adsorption capacities computed from the PSO kinetic model with the experimental adsorption capacity for both the adsorbates together with higher R^2 values illustrated that the kinetics of the adsorption process is compatible with this model. The implication of this outcome is that the adsorption rate is influenced by the concentration of both the adsorbate

and adsorbent. According to the PSO rate constant, AMX is the fastest adsorbing compound compared to TMT. The PSO kinetic model hints that the rate-controlling step was chemisorption between the adsorbates and the adsorbent (27). A similar trend of PSO kinetics has also been reported in the previous studies for the adsorption of pharmaceuticals onto different adsorbents (26,28).

The IPD model was explored to further elucidate the mechanism of adsorption of AMX and TMT onto the MBC. The values of the parameters linked with this model are presented in Table 2. It was observed that the regression of q_t versus $t^{1/2}$ (Figure 11) is non-linear and does not pass through the origin. This deviation signifies that the intraparticle diffusion is not the sole rate-controlling step. Furthermore, the plot indicates the multi-linearity represented by two linear segments, which indicates that the adsorption of both the pharmaceuticals was accompanied by two steps.

The first sharper segment depicts the instantaneous external surface adsorption while the second segment is ascribed to the gradual adsorption stage of intraparticle diffusion and the attainment of equilibrium (27).

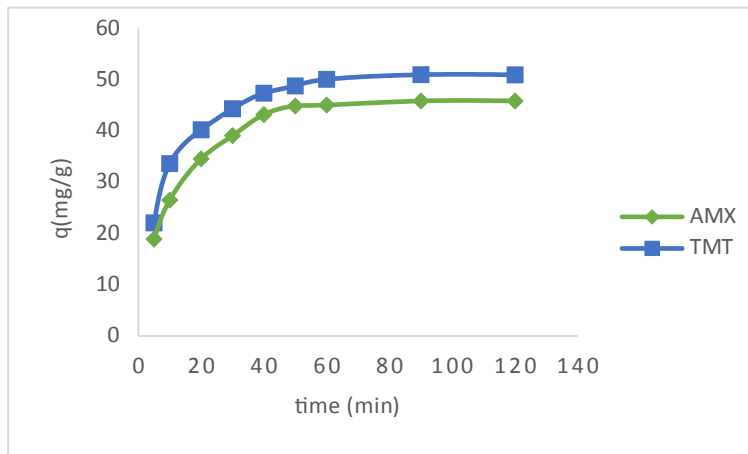


Figure 8: Effect of contact time on the adsorption capacity of MBC towards AMX and TMT (Conditions: contact time = 5-120 min; $C_0 = 60$ mg/L; solution volume = 100 mL; adsorbent weight = 0.1 g; temperature = 303 K).

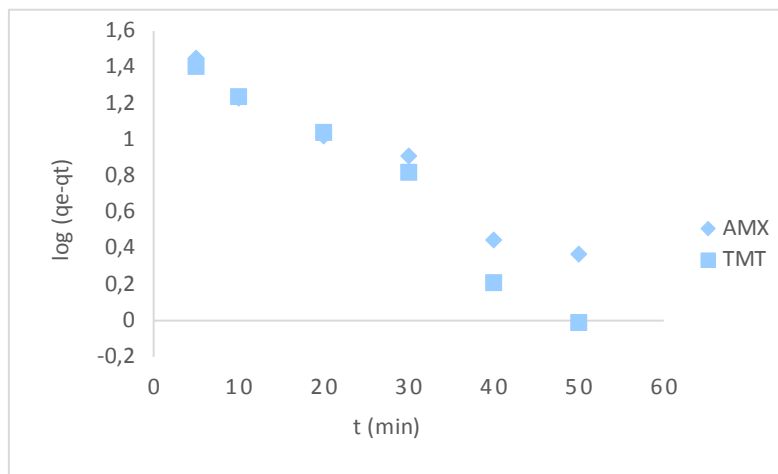


Figure 9: Kinetic data of AMT and TMT adsorption onto MBC adjusted to PFO model (Conditions: contact time = 5-120 min; $C_0 = 60$ mg/L; solution volume = 100 mL; adsorbent weight = 0.1 g; temperature = 303 K).

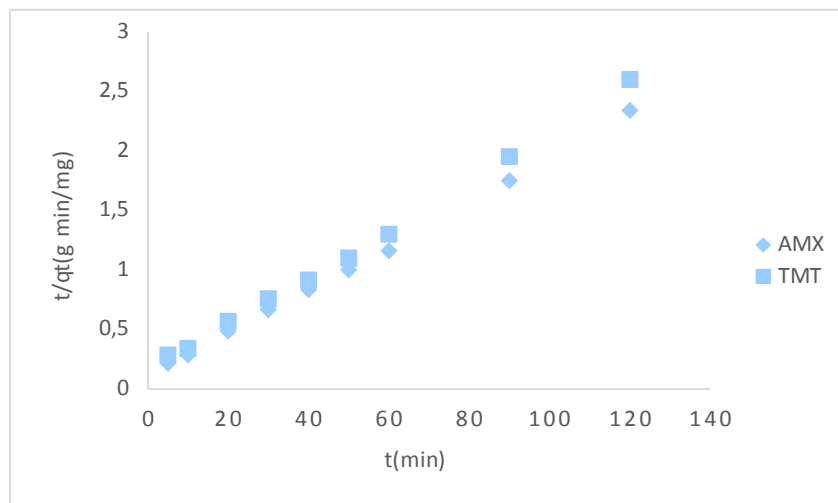


Figure 10: Kinetic data of AMT and TMT adsorption onto MBC adjusted to PSO model (Conditions: contact time = 5-120 min; $C_0 = 60$ mg/L; solution volume = 100 mL; adsorbent weight = 0.1 g; temperature = 303 K).

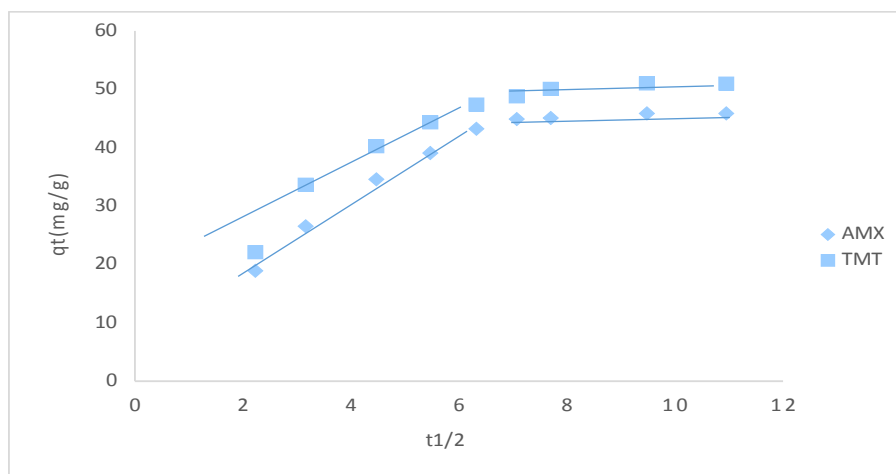


Figure 11: Kinetic data of AMT and TMT adsorption onto MBC adjusted to IPD model (Conditions: contact time = 5-120 min; $C_0 = 60$ mg/L; adsorbent weight = 0.1 g; solution volume = 100 mL; temperature = 303 K).

Adsorption Isotherm

The study of adsorption isotherms is essential to describe how examined adsorbates interact with the target adsorbent surface. Two commonly used models, viz., Langmuir and Freundlich models have been employed to interpret the isotherm data and outcomes so generated are shown in Table 3. The equilibrium data for both adsorbates exhibit appreciable fit to the Langmuir model, attested by highest R^2 and lowest value of SSE and χ^2 . This implies that the adsorption occurred in a homogeneous surface (sites of equal energy and accessibility) leading to the formation of a monolayer of pharmaceuticals on the surface of the MBC that saturates the pores and hampers the transmigration

(25). Furthermore, the value of R_L lies in the range of 0–1, intimating a high degree of favorability of the adsorption process. The maximum adsorption capacities of AMX and TMT calculated from the Langmuir isotherm model are 41.87 and 55.83 mg/g, respectively. This demonstrates the potential of MBC for adsorption of this pharmaceuticals under the employed conditions. On the other hand, the Freundlich model exhibit higher values of SSE and χ^2 for both the adsorbates indicating its unsuitability for inferring adsorption of pharmaceuticals onto the MBC. It is worth mentioning that the affinity for the Langmuir model has been observed in previous studies dealing with AMX and TMT adsorption (26,29).

Table 2: Relevant kinetic fitting parameters for AMX and TMT adsorption onto MBC.

Kinetic model	Parameters	AMX	TMT
Pseudo-first-order	$q_{e,exp}$ (mg/g)	45.10	50.10
	$q_{e,model}$ (mg/g)	33.55	40.98
	k_1 (1/min)	0.06	0.07
	R^2	0.964	0.967
	χ^2	3.98	2.03
Pseudo-second-order	SSE (%)	4.72	3.72
	$q_{e,model}$	44.34	49.75
	$k_2 \times 10^{-3}$ (g/mg min)	4.90	2.88
	R^2	0.999	0.999
	χ^2	0.01	0.007
Intraparticle diffusion	SSE (%)	0.25	0.11
	K_{id}	3.03	3.02
	C	19.10	24.11
	R^2	0.785	0.771

Table 3: Parameters of the fitting to Langmuir and Freundlich models for AMX and TMT.

Isotherm model	Parameters	AMX	TMT
Langmuir	q_{max} (mg/g)	41.87	55.83
	K_L (L/mg)	0.21	0.23
	R_L	0.20	0.68
	R^2	0.994	0.986
	χ^2	0.12	0.14
Freundlich	SSE (%)	0.97	1.04
	K_F (L/mg)	14.53	10.68
	n	2.28	2.50
	R^2	0.969	0.979
	χ^2	2.65	3.96
	SSE (%)	17.20	18.93

Thermodynamic Behavior

In order to examine the nature of the adsorption of pharmaceuticals onto the MBC, the thermodynamic factors, such as the changes in enthalpy ΔH (J/mol), Gibbs free energy ΔG (J/mol), and entropy ΔS (J/mol K) associated with the adsorption process were computed by using Eqs. 15-17:

$$K_d = \frac{q_e}{C_e} \quad (15)$$

$$\Delta G = -RT \ln K_d \quad (16)$$

$$\ln K_d = \frac{-\Delta H}{RT} + \frac{\Delta S}{R} \quad (18)$$

where R denotes the universal gas constant (8.314 J/mol K); T represent the absolute temperature of the

system (K), and the parameter K_d is dimensionless since the unit of R, T and ΔG , are J/mol K, K, and J/mol, respectively. Furthermore, the system's ΔS and ΔH values were estimated from the intercept and gradient of Van't Hoff plot ($\ln K_d$ versus $1/T$), respectively.

Values of ΔG at varying temperatures (303–333 K) evaluated from Eq. (16) and other thermodynamic quantities such as ΔH and ΔS as obtained from Van't Hoff plot (Figure 12) are presented in Table 4. This table revealed that the thermodynamic behavior of both AMX and TMT towards MBC is the same. The negative ΔG values specify that the adsorption phenomenon is thermodynamically feasible under the employed laboratory conditions. The positive values of ΔH and ΔS for both the adsorbates signify that the process is endothermic in nature and accompanied with the increase in the degree of randomness at the adsorbate/adsorbent interface during adsorption (30).

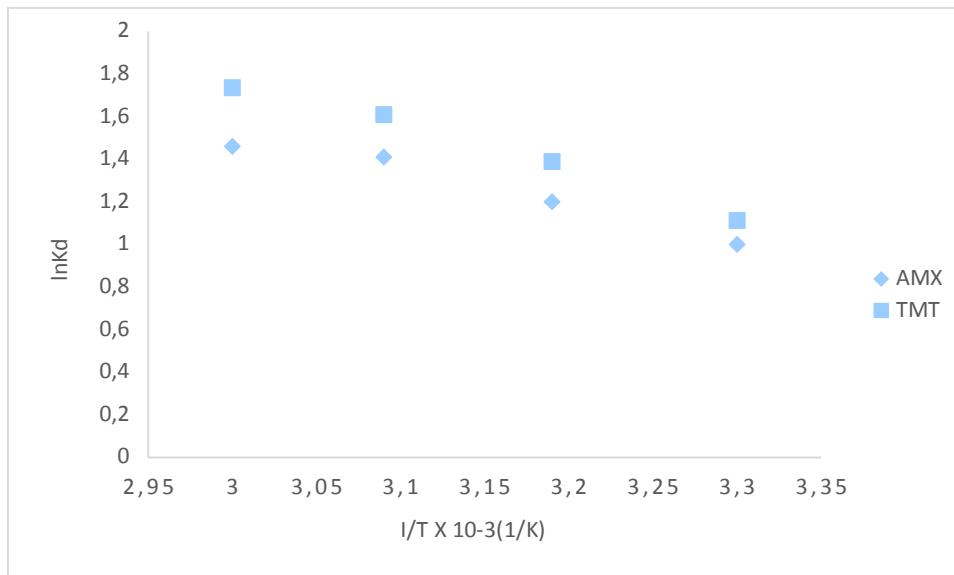


Figure 12: Van't Hoff plot for estimating the ΔH and ΔS of the adsorption system.

Table 4: The thermodynamic parameters for pharmaceuticals adsorption onto MBC.

Adsorbate	ΔH (J/mol)	ΔS (J/molK)	ΔG (J/mol)			
			303K	313K	323K	333K
AMX	13.32	52.42	-2519	-3123	-3786	-4042
TMT	17.47	67.09	-2801	-3615	-4321	-4805

Regeneration and Reuse Analysis

The reusability of adsorbent material is a crucial factor that needs to be taken into cognizance in order to lower the treatment cost as well as mitigate the hazard that might be occasioned by the disposal of pollutant-laden adsorbents. Although there are diverse regeneration strategies, we opted for the chemical method because of its low-cost nature and

zero adsorbent loss. Figure 13 displayed the results in six adsorption cycles. It was apparent that the adsorption amounts were maintained high and relatively stable. The MBC adsorbent retained about 75% of its original adsorption capacity after six reuse cycles. This result verified that the MBC has high economic viability since it could be recycled and reused efficiently.

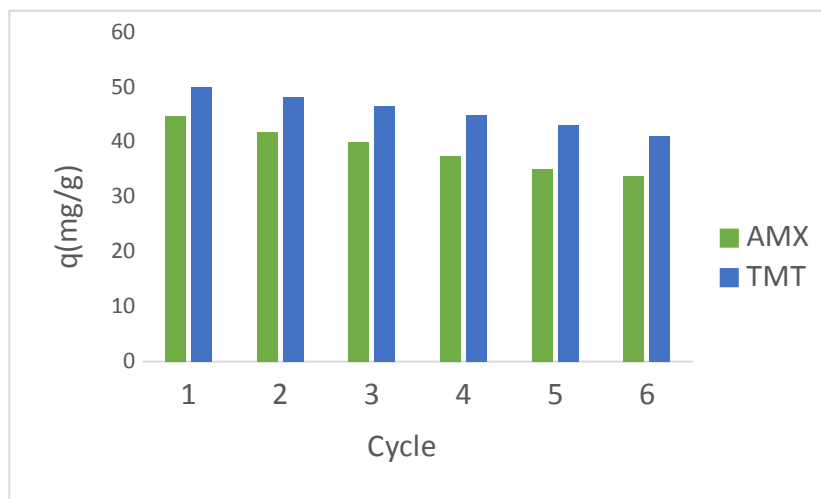


Figure 13: Reuse experiments results.

Density Functional Theory (DFT) Studies

Frontier molecular orbitals (FMOs) analysis

The frontier molecular orbitals are essential descriptors for diagnosing the most reactive site in π -electron systems (31). The values of the computed quantum chemical parameters such as the E_H , E_L , ΔE , A , and I are displayed in Table 5 and the plots generated from the computations are displayed in Figure 14. The value of HOMO energy (E_H) depicts the ability of electron to be donated. When the value of E_H is high, it signifies the ease of donating electron to the vacant orbital of the receptor molecule. When the value of LUMO energy (E_L) is small, this implies that a molecule has a slight resistance to accept electrons. The energy gap (ΔE) is directly linked to the molecular chemical stability. The pharmaceutical AMX exhibited highest energy band gap ($\Delta E = 3.855$ eV) which illustrates its less reactivity and higher stability. The TMT presented the lowest energy gap ($\Delta E =$

3.762 eV) signifying its high reactivity and lowest stability. The determination of parameters like electron affinity and ionization potential is crucial as they are linked to the orbital energies of the LUMO and HOMO, respectively. The higher the value of A , the more the molecule will be a better electron acceptor. The lower the value of I , the more the molecule will be a better electron donor (32).

From Figure 14, it is obvious that the spread of isodensities of LUMOs and HOMOs is different in both the pharmaceuticals. As we can see, for AMX molecule, the HOMO is dispersed over the phenyl ring including its attached oxygen atom and a small part of the side chain attached to the ring. However, the LUMO shows no distribution over the phenyl ring. For TMT, the HOMO density was not spread over the benzene rings while the LUMO was distributed throughout the molecule ring excluding the terminal oxygen atoms attached to the benzene ring.

Table 5: Molecular orbital energies and other properties of studied compounds.

Compounds	E_H (eV)	E_L (eV)	ΔE (eV)	I (eV)	A (eV)
AMX	-5.372	-1.517	3.855	5.372	1.517
TMT	-4.620	-0.858	3.762	4.620	0.858

Global reactivity descriptors

The values of the important global reactivity parameters of the pharmaceuticals under investigation are presented in Table 6. These descriptors are imperative to gain insights about the reactivity and stability of studied molecules. From Table 6, it is obvious that among the two pharmaceuticals, AMX is the chemically hardest having the highest value of η (3.855 eV), whereas TMT has the highest value of σ (0.266 eV) and therefore chemically softer and more reactive. The chemical potential (μ) value gives a clue about the charge transfer within any compound in its lowest energy state. It is clear that AMX has the highest chemical potential value (-3.445 eV). ω is a thermodynamic parameter that plays a vital role in explaining the reactivity of a chemical system. It quantifies the energy changes when a chemical

system becomes saturated by electrons addition. The results indicate that TMT has the lowest ω value (0.997 eV) and is nucleophilic in nature, whereas AMX has the highest value i.e., of 1.539 eV and is electrophilic in nature (32). χ describes the capability of a molecule to draw electrons towards itself in a covalent bond. Thus, AMX possesses higher electronegativity value (3.445 eV) than TMT (2.739 eV); hence it is the best electron acceptor.

According to the results obtained from DFT-based descriptors, TMT molecules are chemically softer (easiness to adsorb) and more reactive in comparison with molecules of AMX. These findings affirm the experimental observations related to the high adsorption capacity of MBC for TMT in comparison with AMX.

Table 6: Global reactivity indices of studied pharmaceuticals.

Property	AMX	TMT
μ (eV)	-3.445	-2.739
η (eV)	3.855	3.762
σ (eV ⁻¹)	0.259	0.266
χ (eV)	3.445	2.739
ω (eV)	1.539	0.997

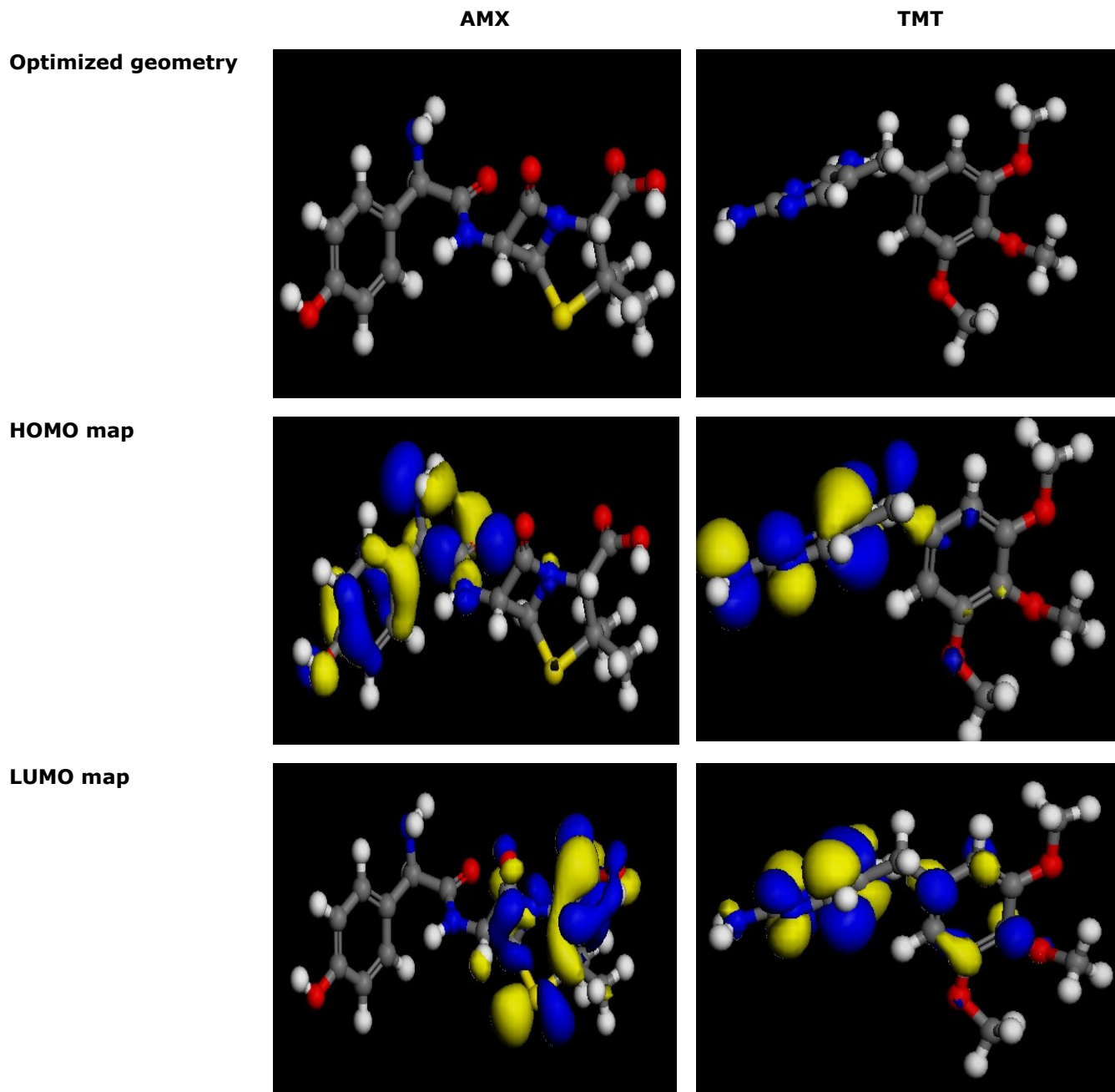


Figure 14: Structural and electronic properties of AMX and TMT.

CONCLUSION

Magnetic biochar derived from *Vitex doniana* nut was fabricated and successfully applied for the effective adsorption of pharmaceuticals from aqueous media. The adsorption behavior of AMX and TMT on MBC adsorbent was investigated. The amount of TMT adsorbed on MBC was higher than that of AMX. Compared to ionic strength, the influence of pH on the adsorption of the adsorbates was significant. The

adsorption kinetics was compatible with the pseudo-second-order model. The adsorption isotherms of AMX and TMT on the magnetic biochar were consistent with the Langmuir model. Thermodynamic investigation showed that the adsorption process was endothermic and spontaneous under studied conditions. The TMT molecules are chemically softer and more reactive in comparison with molecules of AMX. The experimental results of AMX and TMT adsorption onto surface of MBC are in conformity with

the DFT investigation of molecular reactivity of the examined pharmaceuticals. The results showed that the MBC would be a promising material for environmental protection.

REFERENCES

- Ebele AJ, Abou-Elwafa Abdallah M, Harrad S. Pharmaceuticals and personal care products (PPCPs) in the freshwater aquatic environment. *Emerging Contaminants*. 2017 Mar;3(1):1–16. [<DOI>](#).
- Daughton CG. Pharmaceuticals and the Environment (PiE): Evolution and impact of the published literature revealed by bibliometric analysis. *Science of The Total Environment*. 2016 Aug;562:391–426. [<DOI>](#).
- Nazari G, Abolghasemi H, Esmaili M. Batch adsorption of cephalixin antibiotic from aqueous solution by walnut shell-based activated carbon. *Journal of the Taiwan Institute of Chemical Engineers*. 2016 Jan;58:357–65. [<DOI>](#).
- Domínguez JR, González T, Palo P, Cuerda-Correa EM. Removal of common pharmaceuticals present in surface waters by Amberlite XAD-7 acrylic-ester-resin: Influence of pH and presence of other drugs. *Desalination*. 2011 Mar;269(1–3):231–8. [<DOI>](#).
- Sophia A. C, Lima EC. Removal of emerging contaminants from the environment by adsorption. *Ecotoxicology and Environmental Safety*. 2018 Apr;150:1–17. [<DOI>](#).
- Danalioğlu ST, Bayazit ŞS, Kerkez Kuyumcu Ö, Salam MA. Efficient removal of antibiotics by a novel magnetic adsorbent: Magnetic activated carbon/chitosan (MACC) nanocomposite. *Journal of Molecular Liquids*. 2017 Aug;240:589–96. [<DOI>](#).
- Dai Y, Zhang N, Xing C, Cui Q, Sun Q. The adsorption, regeneration and engineering applications of biochar for removal organic pollutants: A review. *Chemosphere*. 2019 May;223:12–27. [<DOI>](#).
- Zhang A, Li X, Xing J, Xu G. Adsorption of potentially toxic elements in water by modified biochar: A review. *Journal of Environmental Chemical Engineering*. 2020 Aug;8(4):104196. [<DOI>](#).
- Hao Z, Wang C, Yan Z, Jiang H, Xu H. Magnetic particles modification of coconut shell-derived activated carbon and biochar for effective removal of phenol from water. *Chemosphere*. 2018 Nov;211:962–9. [<DOI>](#).
- Dadjo C, Assogbadjo AE, Fandohan B, Glèlè Kakaï R, Chakeredza S, Houehanou TD, et al. Uses and management of black plum (*Vitex doniana* Sweet) in Southern Benin. *Fruits*. 2012 Jul;67(4):239–48. [<DOI>](#).
- Ameh PO, Odoh R, Oluwaseye A. Equilibrium study on the adsorption of Zn (II) and Pb (II) ions from aqueous solution onto *Vitex doniana* nut. *Int J Modern Chem*. 2012;3(2):82–97.
- Atolaiye BO, Babalola JO, Adebayo MA, Aremu MO. Equilibrium modeling and pH-dependence of the adsorption capacity of *Vitex doniana* leaf for metal ions in aqueous solutions. *African Journal of Biotechnology*. 2009;8(3). [<URL>](#).
- Florey K. *Analytical profile of drug substances*. Academic Press; 1978.
- Kerkez-Kuyumcu Ö, Bayazit ŞS, Salam MA. Antibiotic amoxicillin removal from aqueous solution using magnetically modified graphene nanoplatelets. *Journal of Industrial and Engineering Chemistry*. 2016 Apr;36:198–205. [<DOI>](#).
- Kakavandi B, Rezaei KR, Jonidi JA, Esrafiy A, Gholizadeh A, Azari A. Efficiency of powder activated carbon magnetized by Fe₃O₄ nanoparticles for amoxicillin removal from aqueous solutions: Equilibrium and kinetic studies of adsorption process. 2014; 7(1): 21–34. [<URL>](#).
- Bakatula EN, Richard D, Neculita CM, Zagury GJ. Determination of point of zero charge of natural organic materials. *Environ Sci Pollut Res*. 2018 Mar;25(8):7823–33. [<DOI>](#).
- Tran HN, You S-J, Hosseini-Bandegharai A, Chao H-P. Mistakes and inconsistencies regarding adsorption of contaminants from aqueous solutions: A critical review. *Water Research*. 2017 Sep;120:88–116. [<DOI>](#).
- Ouasfi N, Zbair M, Bouzikri S, Anfar Z, Bensitel M, Ait Ahsaine H, et al. Selected pharmaceuticals removal using algae derived porous carbon: experimental, modeling and DFT theoretical insights. *RSC Adv*. 2019;9(17):9792–808. [<DOI>](#).
- Chen Y, Shi J, Du Q, Zhang H, Cui Y. Antibiotic removal by agricultural waste biochars with different forms of iron oxide. *RSC Adv*. 2019;9(25):14143–53. [<DOI>](#).
- Cornell RM, Schwertmann U. *The iron oxides: structure, properties, reactions, occurrences, and uses*. 2nd, completely rev. and extended ed ed.

Weinheim: Wiley-VCH; 2003. 664 p. ISBN: 978-3-527-30274-1.

21. Liu P, Li H, Liu X, Wan Y, Han X, Zou W. Preparation of magnetic biochar obtained from one-step pyrolysis of *salix mongolica* and investigation into adsorption behavior of sulfadimidine sodium and norfloxacin in aqueous solution. *Journal of Dispersion Science and Technology*. 2020 Jan 28;41(2):214–26. [<DOI>](#).
22. Yunusa U, Bishir U, Bashir IM. Experimental and quantum chemical investigation for the single and competitive adsorption of cationic dyes onto activated carbon. *Alg J Eng Technol*. 2021 Feb 4;4:7–21. [<DOI>](#).
23. Devi P, Saroha AK. Simultaneous adsorption and dechlorination of pentachlorophenol from effluent by Ni-ZVI magnetic biochar composites synthesized from paper mill sludge. *Chemical Engineering Journal*. 2015 Jul;271:195–203. [<DOI>](#).
24. Santhosh C, Daneshvar E, Tripathi KM, Baltrėnas P, Kim T, Baltrėnaitė E, et al. Synthesis and characterization of magnetic biochar adsorbents for the removal of Cr(VI) and Acid orange 7 dye from aqueous solution. *Environ Sci Pollut Res*. 2020 Sep;27(26):32874–87. [<DOI>](#).
25. Alnajrani MN, Alsager OA. Removal of Antibiotics from Water by Polymer of Intrinsic Microporosity: Isotherms, Kinetics, Thermodynamics, and Adsorption Mechanism. *Sci Rep*. 2020 Dec;10(1):794. [<DOI>](#).
26. Berges J, Moles S, Ormad MP, Mosteo R, Gómez J. Antibiotics removal from aquatic environments: adsorption of enrofloxacin, trimethoprim, sulfadiazine, and amoxicillin on vegetal powdered activated carbon. *Environ Sci Pollut Res*. 2021 Feb;28(7):8442–52. [<DOI>](#).
27. Ahmed M, Mashkoo F, Nasar A. Development, characterization, and utilization of magnetized orange peel waste as a novel adsorbent for the confiscation of crystal violet dye from aqueous solution. *Groundwater for Sustainable Development*. 2020 Apr;10:100322. [<DOI>](#).
28. Mokhati A, Benturki O, Bernardo M, Kecira Z, Matos I, Lapa N, et al. Nanoporous carbons prepared from argan nutshells as potential removal agents of diclofenac and paroxetine. *Journal of Molecular Liquids*. 2021 Mar;326:115368. [<DOI>](#).
29. Liu H, Hu Z, Liu H, Xie H, Lu S, Wang Q, et al. Adsorption of amoxicillin by Mn-impregnated activated carbons: performance and mechanisms. *RSC Adv*. 2016;6(14):11454–60. [<DOI>](#).
30. Yunusa U, Usman B, Ibrahim M. Modeling and Regeneration Studies for the Removal of Crystal Violet Using *Balanites aegyptiaca* Seed Shell Activated Carbon. *Journal of the Turkish Chemical Society Section A: Chemistry*. 2020 Dec 29;197–210. [<DOI>](#).
31. Umar Y, Abu-Thabit N, Jerabek P, Ramasami P. Experimental FTIR and theoretical investigation of the molecular structure and vibrational spectra of acetanilide using DFT and dispersion correction to DFT. *J Theor Comput Chem*. 2019 Mar;18(02):1950009. [<DOI>](#).
32. Khan SA, Rizwan K, Shahid S, Noamaan MA, Rasheed T, Amjad H. Synthesis, DFT, computational exploration of chemical reactivity, molecular docking studies of novel formazan metal complexes and their biological applications. *Appl Organometal Chem [Internet]*. 2020 Mar [cited 2021 Oct 29];34(3).5444, 1-24. [<DOI>](#).

